Electrochemical Impedance Spectroscopy of Polyelectrolyte Multilayer Modified Electrodes

ARTICLE *in* THE JOURNAL OF PHYSICAL CHEMISTRY B · OCTOBER 2004

Impact Factor: 3.3 · DOI: 10.1021/jp0466845

Electrochemical Impedance Spectroscopy of Polyelectrolyte Multilayer Modified Electrodes

Sérgio V. P. Barreira,*,† Vladimir García-Morales,‡ Carlos M. Pereira,† José A. Manzanares,‡ and Fernando Silva†

Departamento de Química da Faculdade de Ciências da Universidade do Porto, Rua do Campo Alegre, 687, 4169-007 Porto, Portugal, and Departament de Termodinàmica, Universitat de València, E-46100 Burjassot, Spain

Received: July 26, 2004; In Final Form: September 3, 2004

Electrochemical impedance spectroscopy, Fourier transform infrared reflection−absorption spectroscopy, and cyclic voltammetry were employed to characterize polyelectrolyte multilayers (PEMs) fabricated with poly(styrenesulfonate) as the polyanion and the polypeptides poly-L-histidine, poly-L-lysine, and poly-L-arginine as polycations. The layer-by-layer electrostatic assembly was produced onto alkanethiol-modified gold surfaces. The frequency response reveals that the effect of the number of layers seems to be related to a progressive reduction in the active area of the PEM-modified electrodes. The active area after the deposition of seven layers can be lower than 10% of its original value. The film surface is then inhomogeneous with respect to the transport of the electroactive species and has spots through which transport is quite favored. These structural features of the PEM have been taken into account in the theoretical model of ion transport and very good agreement with the experimental impedance results has been found.

Introduction

Polyelectrolyte multilayers (PEMs) assembled by alternate adsorption of oppositely charged polyelectrolytes have been widely studied as a means to obtain films with desired functionalities.[1−9] Research with these multilayers have revealed, for example, that the sequential adsorption occurs because of charge overcompensation after each layer deposition,[10−12] and that there exists a threshold value for surface charge density below which assembly cannot propagate.[13,14] Moreover, the layers are interpenetrated,[15] and the pH and ionic strength of the deposition solutions can be used to control the amount deposited, the thickness, and the roughness of the multilayer.[16−18]

Mass transport in PEMs has been addressed in recent studies.[19−28] By using PEM-modified electrodes, it has been discovered that, although the multilayers are very permeable to the monovalent or divalent ions of the supporting electrolyte, the permeability toward heavily charged electroactive ions such as $[Fe(CN)_6]^{3-}$ and $[Ru(NH_3)_6]^{3+}$ decreases rapidly with the number of layers. Furthermore, multilayers terminated with a polycation layer are more permeable to negatively charged ion probes. Some authors[23,24] attributed the decrease in permeability with the number of layers to a reduction in the active area of the electrode.

Recently, Schlenoff et al.,[26−28] on the basis of the observed increases of limiting current with increases in the external salt concentration, proposed that the diffusion of the probe ion in the film is described as hopping between "exchange sites" created within the film by the supporting electrolyte. The strong attenuation of the current is explained as a combination of a low diffusion coefficient and a low concentration of the electroactive ion in the film. The decrease in permeability with the number of layers is attributed to a decrease in the concentration gradient in the film due to an increase in film thickness. The enhanced transport of negatively charged ions through multilayers bearing positive surface charge is thought to be due to a Donnan-enhanced concentration in the multilayer.

In the present work electrochemical impedance spectroscopy (EIS) and cyclic voltammetry (CV) were employed to investigate the electroactivity of the redox couple $[Fe(CN)_6]^{3-}/[Fe(CN)_6]^{4-}$ at electrodes coated with polyelectrolyte multilayers containing poly(styrenesulfonate) as the polyanion and the poly(amino acids) poly-L-histidine ($pK_a \sim 7$), poly-L-lysine ($pK_a \sim 10$), and poly-L-arginine ($pK_a \sim 12$) as the polycations (Figure 1). Impedance measurements have been previously utilized in the characterization of PEM-modified electrodes by other researchers;[23−25] however, they were analyzed on the basis of the Randles circuit. This is an inappropriate equivalent circuit because the mass transport cannot be fully described by the Warburg impedance.[29−35] Significant deviation from semi-infinite linear diffusion is expected either when the electroactivity is attributed to the existence of bare areas distributed on the film surface[29−34] or when it is treated as a permeable membrane.[26−28,35] In the first case the theoretical models available generally assume an evenly spaced array of disk-shaped bare areas embedded in an insulating plane behaving as a array of microelectrodes. The estimation of the parameters controlling the array of active sites for this model is well demonstrated from EIS measurements, for example, for monolayers of alkanethiols on gold electrodes exhibiting residual electroactivity due to pinholes in the monolayer having radii of 0.1−10 μm and separations of 1−100 μm.[33,36,37] We provide below an extension of this model to account for the change in film structure that accompanies the assembly of successive layers. The diffusion impedance based on this capillary membrane model (CMM) is expected to give the best approximate description if the layer-by-layer (LBL) assembly originates an inhomogeneous film. Contrarily, if there are no privileged paths

* To whom correspondence should be addressed. Phone: (351) 22 6082934. Fax: (351) 22 6082959. E-mail: spbarrei@fc.up.pt.
† Universidade do Porto.
‡ Universitat de València.

10.1021/jp0466845 CCC: $27.50
Published on Web 10/20/2004

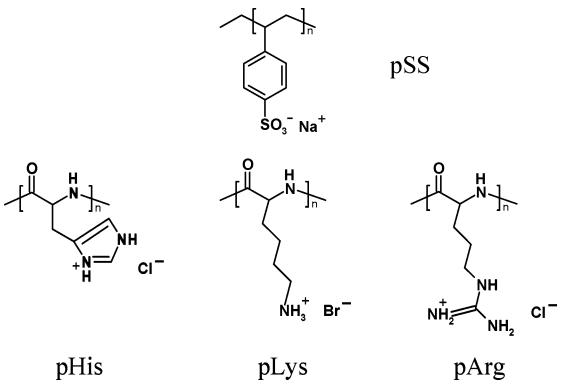

Figure 1. Chemical structures of the monomer units of poly(sodium 4-stryrenesulfonate) (pSS), poly(L-histidine hydrochloride) (pHis), poly-(L-lysine hydrobromide) (pLys), and poly(L-arginine hydrochloride) (pArg).

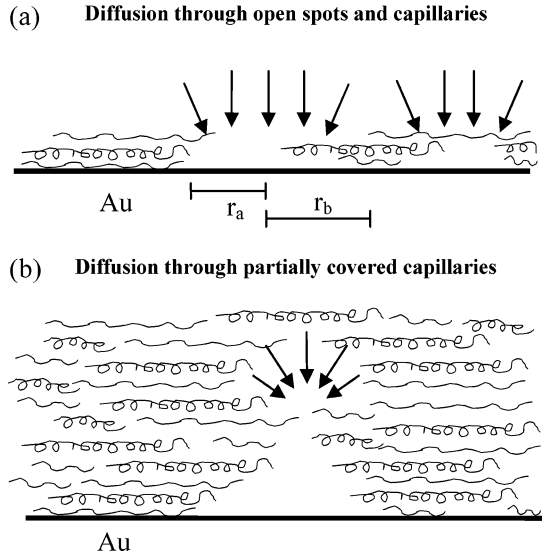

Figure 2. Electrochemical active site configuration at two stages of film growth and their associated diffusion profiles.

for the charge transport, the multilayer can be described with a homogeneous membrane model (HMM).[26]

Electrochemical Diffusion Impedance of the PEM-Modified Electrode

I. The Capillary Membrane Model (CMM). This model considers that the effect of the LBL assembly is the progressive reduction of the active area of the electrode. When only a few layers have been deposited, the film is very porous. There may exist electrode areas that are either bare or covered by only one or two layers. The effective coverage of the electrode for these films is small. Figure 2a illustrates this situation. The bare areas may correspond, for example, to those where there was no self-assembly of the alkanethiol. It is known that short chain (number of methylene units < 9) alkanethiols originate disordered monolayers with pinholes, that is, uncovered electrode areas.[38,39] These pinholes may persist during the sequential assembly of the polyelectrolyte layers, although their area is progressively reduced and they tend on the average to be further apart from each other as more layers are added. Eventually, after a certain number of layers, most of these pinholes become very narrow or covered by polyelectrolyte. At this stage the remaining electroactivity may still be associated with the previous opened spots because these continue to be sites were the film is less dense, but now the species has to diffuse through the external layers before reaching a capillary. This situation is depicted in Figure 2b.

The above description may imply significant deviations from semi-infinite linear diffusion.[29−34] In fact, diffusion to and from the active sites becomes more spherical with the decrease in the radius of the active sites and with the increased coverage.[32,33] In the situation illustrated in Figure 2b, which is expected for a high number of layers, the nonlinear diffusion region is located in the film.

Partitioning effects (due to hydrophobic and electrostatic interactions) can be taken into account by considering that the concentration of species k ($k = 1$ for $[Fe(CN)_6]^{4-}$ and $k = 2$ for $[Fe(CN)_6]^{3-}$) in the vicinity of the film surface c_k^f is given by $c_k^f = K_k c_k^s$, where c_k^s is its concentration in the bulk solution. In the case of high coverage the partition coefficient K_k accounts for the partitioning between the external solution and the compact regions close to the capillaries. Furthermore, due to the different nature of the paths as the coverage increases, the effective diffusion coefficient D_k^f for transport through the film of species k departs from that in the external solution D_k^s in a factor D_R, i.e., $D_k^f \equiv D_R D_k^s$.

The diffusion impedance of partially blocked electrodes is often modeled by assuming that the ensemble of active sites behaves as an ideal array of microelectrodes.[31,33] These models can be adapted for PEM-modified electrodes having capillaries (or preferential transport paths) and areas through which transport is hindered or very unfavorable. The diffusion impedance for a regular array (uniform size and separation) of circular active areas of radius r_a distributed on an inert surface in contact with a solution is[31,33]

$$Z_d^{(c)} = \sum_k \frac{\sigma_k^{(c)}}{\sqrt{\omega}}\left[1 + \frac{\theta}{(1-\theta)}\left(\frac{[1+(q_k/\omega)^2]^{1/2} + q_k/\omega}{1+(q_k/\omega)^2}\right)^{1/2} + j + \frac{j\theta}{(1-\theta)}\left(\frac{[1+(q_k/\omega)^2]^{1/2} - q_k/\omega}{1+(q_k/\omega)^2}\right)^{1/2}\right] \quad (1)$$

where

$$\sigma_k^{(c)} = \frac{RT}{n^2F^2A\sqrt{2D_k^f c_k^f}} \quad (2)$$

and

$$q_k = \begin{cases} \dfrac{2D_k^f}{r_b^2\theta(1-\theta)\ln(1+0.27/\sqrt{1-\theta})} & 1-\theta > 0.1 \\ \dfrac{D_k^f}{0.36r_a^2} & 1-\theta \le 0.1 \end{cases} \quad (3)$$

In eqs 1−3, R is the ideal gas constant, T is the temperature, F is the Faraday constant, n is the number of electrons involved in the electrode reaction ($n = 1$ in our case), A is the electrode area, j is $\sqrt{-1}$, and ω is the angular frequency. The coverage θ and the radius r_b of inactive area surrounding the active site are related by the following relation

$$1 - \theta = \frac{r_a^2}{r_b^2} \quad (4)$$

II. Homogeneous Membrane Model (HMM). The PEM has also been modeled as a homogeneous membrane where the increase in the number of layers leads to an increase in the thickness L of the film,[26−28] a decrease in the concentration gradient, and then a decrease in the current. This tendency, for the decrease in the permeability with the number of layers may not occur when the last layer deposited and the electroactive species have opposite charge. In this case the decrease in concentration gradient associated with the increase in film thickness may be compensated by an enhanced inclusion of the species in the film. The film−solution interface is considered to be in electrochemical equilibrium. The diffusion coefficient D_k^f and the partition coefficient K_k of species k are allowed to vary with the number of layers. This model leads to the diffusion impedance (see Appendix)

$$Z_d^{(m)} = \sum_k \frac{\sigma_k^{(m)}}{\sqrt{j\omega}} \frac{\tanh(a_k\sqrt{\omega}) + b_k}{1 + b_k \tanh(a_k\sqrt{\omega})} \quad (5)$$

where a_k, b_k, and $\sigma_k^{(m)}$ are defined in eqs A8, A9, and A11.

Experimental Section

I. Materials. The chemicals, cysteamine (Fluka), poly(sodium 4-styrenesulfonate) (Mw, 70 000) (pSS, Aldrich), poly(L-histidine hydrochloride) (Mw, 15 800) (pHis, Sigma), poly(L-lysine hydrobromide) (Mw, 32 600) (pLys, Sigma), poly(L-arginine hydrochloride) (Mw, 38 300) (pArg, Sigma), potassium hexacyanoferrate(III) (Merck, pa quality), potassium hexacyanoferrate-(II) (Merck, pa quality), acetic acid 100% (Pronalab, pa quality), sodium acetate trihydrate (Merck, pa quality), Na_2SO_4 anhydrous (Merck, suprapur), and $HClO_4$ 70% (Merck, suprapur), were all used as received. Millipore filtered water (resistivity >18 MΩ cm) was used to prepare all aqueous solutions and for rinsing.

Commercial gold slides (5 nm Cr and 100 nm Au) were purchased from Evaporated Metal Films (Ithaca, NY) and used as substrates in the FT-IRRAS measurements after being degreased by a brief wash with acetone and then cleaned by soaking in a 3:1 mixture of concentrated sulfuric acid and hydrogen peroxide (30%) (piranha solution) for about 1 min, followed by thorough washing with large amounts of Millipore water. ***Caution!*** *Piranha solution is corrosive and reacts violently with organic materials.*

II. Synthesis of the Polyelectrolyte Films. The sequential assembly of the polyelectrolyte multilayer was promoted by a positively charged cysteamine monolayer self-assembled on the gold surface. The monolayer was chemisorbed onto the gold surfaces from a 1 mM ethanolic solution for at least 10 h. After self-assembly the surface was rinsed with ethanol and water, and dried in a stream of nitrogen. The multilayers, up to 10 layers, were obtained by alternately dipping the modified gold surface in solutions (1 mg/mL, in CH_3COOH/CH_3COONa 0.1 M, pH 4.5) of pSS and polycation for 10 min. After the assembly of each new layer, the surface was rinsed with water and dried in a stream of nitrogen.

III. Fourier Transform Infrared Reflection−Absorption Spectroscopy (FT-IRRAS). The FT-IRRAS spectra in the mid-IR region were recorded on a Perkin-Elmer 2000 FTIR with its sample area modified to accommodate an external reflection sampling geometry. The spectra were obtained using the p-polarized component of the radiation at an incident angle of approximately 77° relative to the surface normal, with a narrow-band MCT detector liquid nitrogen cooled. The sample area was purged by dry air delivered from a CDA series MTI-Puregas purge gas generator. Each spectrum was obtained with a resolution of 4 cm^{-1}. A bare gold slide, rigorously cleaned according to the procedure described in the materials section, was used as a background surface. Background spectra consisting of 200 averaged scans were taken before collecting each sample spectra. The sample spectra reported consists of about 1000 averaged scans.

IV. Electrochemical Measurements. The assembly of a new multilayer film on the electrode was preceded by the following cleaning steps. First, the electrode was treated with a fresh piranha solution for 5 min. Through FT-IRRAS measurements we were able to confirm that this operation leads to a complete removal of the film held to the surface by electrostatic interactions. The second step consisted of polishing the electrode with alumina slurry on a felt pad (Buhler) until mirror finish. This was followed by ultrasonication and thorough water rinsing. Finally, a CV of the electrode in $HClO_4$ 0.1 M between −0.4 and +1.5 V (vs Ag/AgCl) was obtained to ensure that the Au surface was effectively cleaned.

Electrochemical measurements were conducted using a three-electrode cell with an Ag/AgCl (3 M KCl) reference electrode (with a Luggin tip) and a bright platinum grid of large area as counter electrode. The working electrode was the modified gold electrode (gold disk, geometrical area = 3.14 mm^2). Na_2SO_4 (0.1 M) was employed as supporting electrolyte. The measurements were carried out in deoxygenated aqueous solutions, and the cell was kept under flowing nitrogen during the measurements.

For each multilayer CV measurements were immediately followed by EIS measurements. CV measurements were performed using a Solartron potentiostat (Model 1287). For EIS measurements the potentiostat was connected to a Solartron frequency response analyzer (Model 1250). The EIS measurements were made in the frequency range from 15 kHz to 100 mHz with frequencies logarithmically spaced (10 points per decade) using a 10 mV peak to peak sinusoidal perturbation with the electrode held at the dc formal potential of the system (0.160 V).

It was found, for the thicker multilayers, that an increasing number of scans were needed before a stable CV was obtained. This may be attributed to the swelling of the multilayers by supporting electrolyte;[24] i.e., the multilayer is evolving from "intrinsic" to increasing "extrinsic" compensation. These concepts were introduced by Schlenoff[40,41] and make reference to whether the charge within the multilayer is compensated by small mobile ions (extrinsic compensation) or by complexation of the polyelectrolytes (intrinsic compensation).

Results

I. FT-IRRAS Characterization. Figure 3 shows the FT-IRRAS spectra for the several layers of the films studied. These spectra show that the LBL assembly is successful in every case. The most prominent features, common to all spectra, are the amide bands of the poly(amino acids) amide I (∼1665 cm^{-1}) and amide II (∼1540 cm^{-1}) and the bands attributed to the pSS at 1200 cm^{-1} ($\nu_{as}(SO_3^-)$), 1127 and 1009 cm^{-1} (ring deformation vibrations), and 1036 cm^{-1} ($\nu_s(SO_3^-)$) (see detailed band assignment of the FT-IRRAS spectra in the Supporting Information).

The absorbance values increase almost linearly, suggesting a similar trend for the mass of polymer deposited. Sometimes the linear increase in multilayer mass is accompanied by a

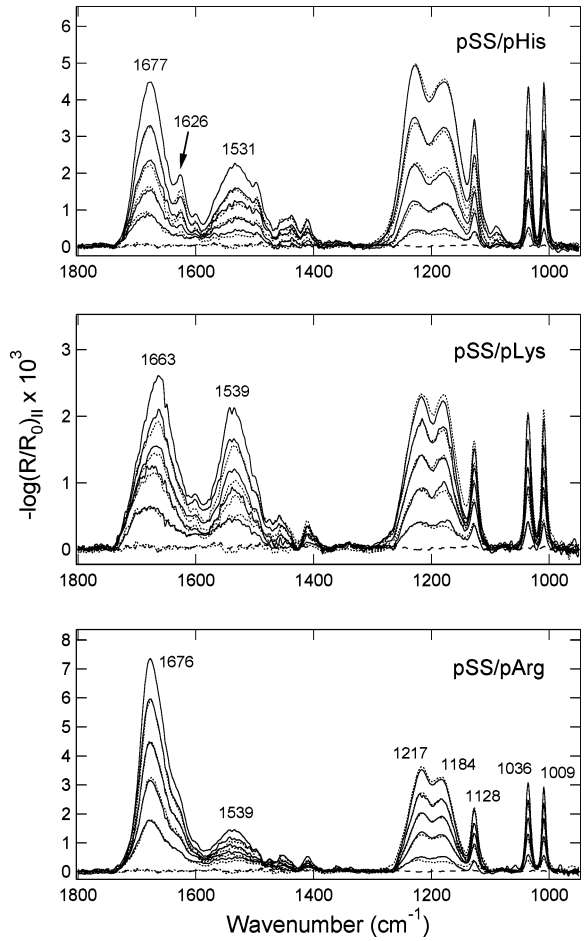

Figure 3. FT-IRRAS spectra of the pSS/poly(amino acid) multilayer films, assembled on a cysteamine-modified gold surface (dashed line spectrum). The dotted lines correspond to films terminated with a pSS layer.

nonlinear increase in multilayer thickness namely for solvent swollen multilayers.[24,25] The spectra also reveal that the intensity of the pSS bands depend on the nature of the polycation. The difference is accentuated slowly as the number of layers increases. For example, the intensity of the broad band at 1200 cm^{-1} for the films with 10 layers is of 0.0040, 0.0019, and 0.0030 au for the pSS/pHis, pSS/pLys, and pSS/pArg films, respectively. These intensities suggest that the amount of pSS contained in each film is on the order pSS/pHis > pSS/pArg > pSS/pLys.

Because at the pH of deposition all the polyelectrolytes used are fully ionized, the differences observed may be attributed to the influence of hydrophobic and van der Waals interactions in the LBL assembly process.[42] These interactions are expected to be stronger between pSS and pHis because the histidine residue and the benzenesulfonate groups of pSS have aromatic character. The fact that the guanidino group of pArg has a planar geometry with delocalized charge should also favor better interaction between these groups and the benzenesulfonate groups of pSS, thus leading to an increased amount of pArg deposited when compared to pLys.[43] The difference in the hidrophobicity of the pArg and pLys tails may also contribute to the trend observed.

II. Electrochemical Measurements. Figures 4−9 show the impedance spectra in the form of Nyquist diagrams and the CVs corresponding to the reaction of $[Fe(CN)_6]^{3-/4-}$ at the PEM-modified electrodes. As it is clearly noticed, the multilayer buildup has a marked influence on the electrode response. We use this fact to extract information about the transport in the PEMs. Research carried using other polyelectrolytes led to similar CV and EIS results.[23−25,44]

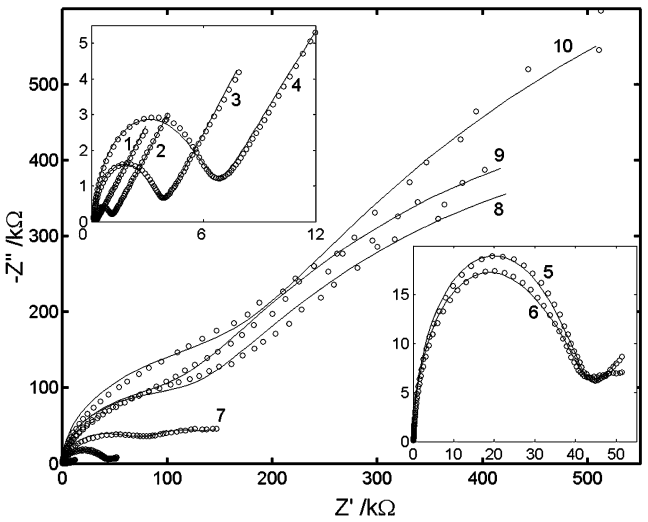

Figure 4. Nyquist diagrams of 5 mM $[Fe(CN)_6]^{3-/4-}$ in 0.1 M Na_2SO_4 at the PEM-modified gold electrode (pSS/pHis films). The number of layers *N* is indicated close to the curves. The experimental data are represented by circles and the solid lines represent theoretical fits.

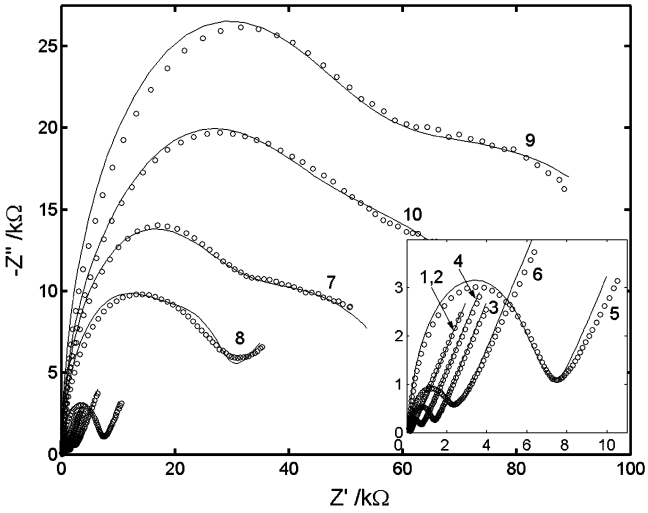

Figure 5. Same as Figure 4 for pSS/pLys films.

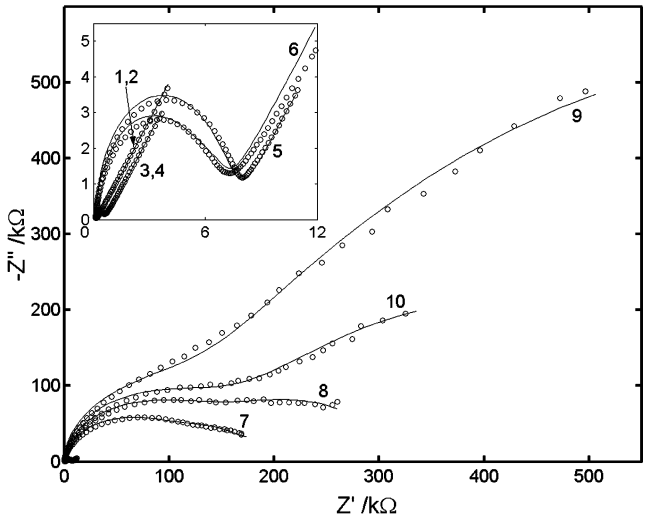

Figure 6. Same as Figure 4 for pSS/pArg films.

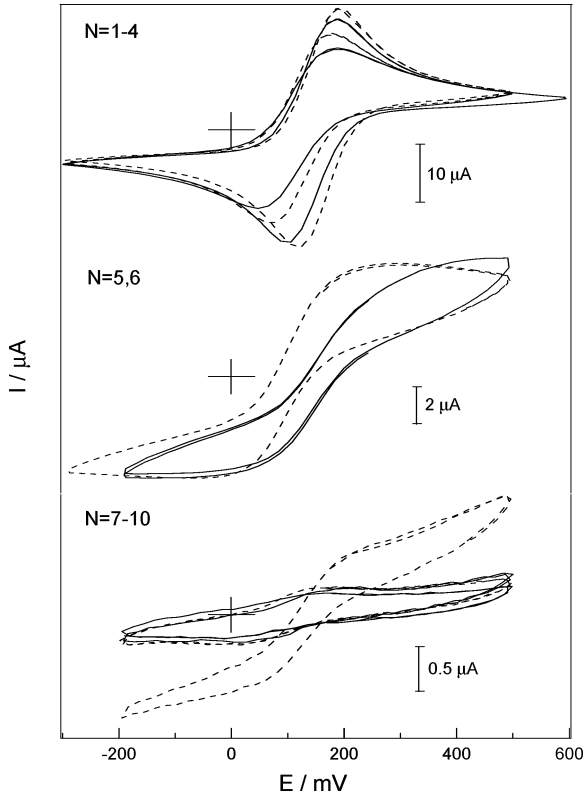

Figure 7. Cyclic voltammograms of 5 mM $[Fe(CN)_6]^{3-/4-}$ in 0.1 M Na_2SO_4 at the PEM-modified gold electrode (pSS/pHis films), scan rate 50 mV s^{-1}. The number of layers *N* is indicated close to the curves. The dashed lines correspond to films terminated with a pSS layer.

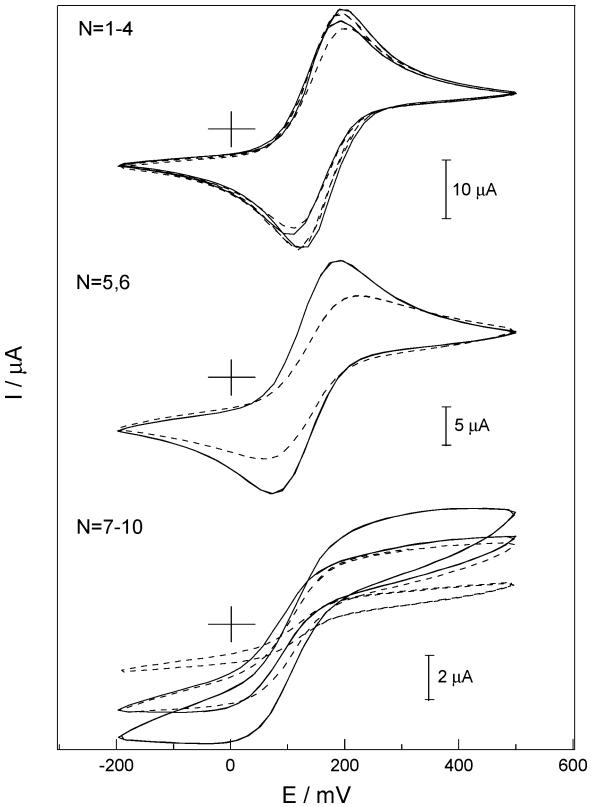

Figure 8. Same as Figure 7 for pSS/pLys films.

The essential features of the impedance spectra do not change during the deposition of the first four layers for the pSS/pHis and six layers for the pSS/pLys and pSS/pArg films (insert in Figures 4-6). The Nyquist diagrams, except for the cysteamine monolayer, show a semicircle in the high-frequency region and a straight line of approximately unit slope at low frequencies. The semicircle is usually associated with resistance and capacitance elements in parallel, and the straight line at low frequencies with mass transport by linear diffusion. For the cysteamine monolayer the only impedance is due to mass transport, so only the straight line of unit slope is seen in the Nyquist diagram (not shown).

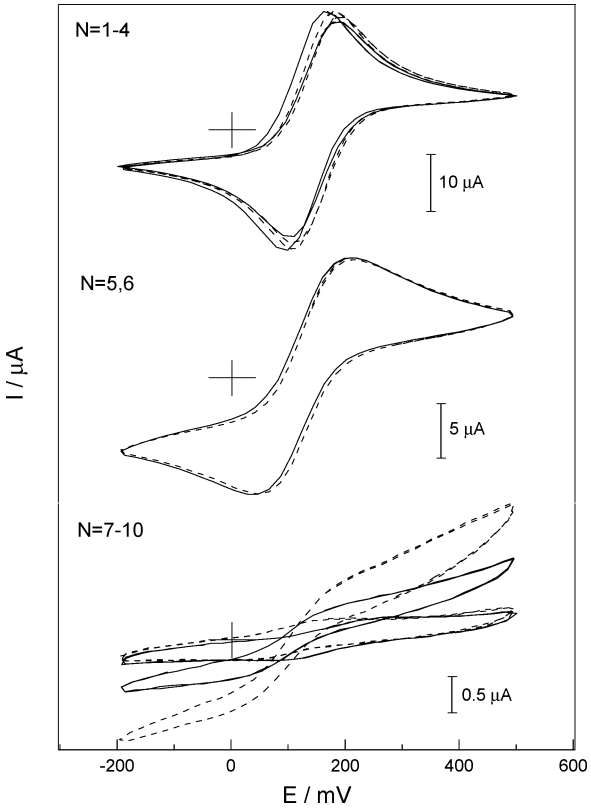

Figure 9. Same as Figure 7 for pSS/pArg films.

For the first layers, the global trend is the nonlinear increase in the diameter of the semicircle as the number of deposited layers increases. This is more pronounced for the pSS/pHis film. The largest increase in impedance per bilayer is measured with this film, followed by the pSS/pArg film.

An increased permeability for positively terminated multilayers has been reported when the electroactive probe is negatively charged.[25,26,45] For the multilayers studied here, this is only observed for the pSS/pLys case. The impedance values decrease after the assembly of the pLys layers. For the pSS/pHis films there is an increase in the impedance values upon deposition of each pHis layer whereas it is observed that the pArg-terminated films (particularly for $N < 7$) offer almost the same impedance as the precedent pSS-terminated ones.

This diverse behavior is also noticed in the cyclic voltammograms of Figures 7−9. With the addition of the polycationic layer the current decreases in the case of pHis, increases in the case of pLys and remains almost unchanged in the case of pArg. The global trend though is a small decrease in peak current, with the number of layers, and is more pronounced in the case of the pSS/pHis multilayer. An increase in peak separation is also noticed, namely with the pSS/pHis multilayer.

The assembly of the fifth layer in the pSS/pHis multilayer, seventh layer in the pSS/pLys and pSS/pArg multilayers, produces a dramatic change in the EIS spectra. A much larger increase is observed in the high-frequency semicircle, and the

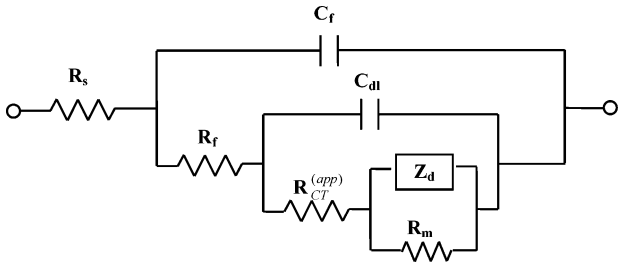

Figure 10. Equivalent circuit for the PEM-modified electrode where R_s is the solution resistance, C_f is the film capacitance, R_f is the film resistance, C_{dl} is the double layer capacitance associated with metal surface, $R_{CT}^{(app)}$ is the apparent charge-transfer resistance, R_m is the resistance representing ohmic conduction in the film, and Z_d is the diffusion impedance.

straight line of unit slope at low frequencies commonly associated with semiinfinite linear diffusion in the solution gives place to what seems to be a second semicircle. The subsequent layers cause additional increases in the high-frequency semicircle (although not so markedly) and in the impedance at lower frequencies.

These changes are also clearly detected in the CVs, because contrary to what was observed for the first layers, significant changes in the EIS spectra occur at low frequencies, i.e., in the time scale of the CVs, suggesting alterations in the way mass transport is carried out. Besides the pronounced reduction in the currents, the CVs became plateau-shaped, as shown in Figures 7−9. Another characteristic superimposed to this change for $N \geq 5$ is a ramp-like character of the CVs. This phenomenon has been previously reported[26] and attributed to ohmic conduction via electron hopping. If still more layers are added, the ramps tend to disappear, but the CVs keep their plateau shape.

Discussion

The EIS results have been analyzed using the equivalent circuit in Figure 10, which has been previously used to model the frequency response of coatings,[46] electrodes modified with polymer films[47] and SAMs.[48] The elements R_f and C_f represent multilayer resistance and capacitance, respectively. The resistance R_f depends on the film thickness, ion content and mobility.[48,49] The capacitance C_f takes into account the double layer due to the charge overcompensation phenomenon.[13,14] Z_d is the diffusion impedance given by eq 1 or 5. The inclusion of the resistance R_m in the equivalent circuit accounts for an ohmic conduction mechanism (parallel to diffusion) and is consistent with the observation of the ramp like behavior in some CVs for $4 \leq N \leq 10$ as well as with the observations by other authors.[26] The theoretical impedances for this equivalent circuit were calculated using Matlab. The diffusion impedance evaluated from the CMM yields realistic values for the transport parameters of the three different films under study. On the contrary, the HMM turns out to be inadequate for films with less than eleven layers. We discuss in detail below the results obtained.

I. Capillary Membrane Model. It is well-known that the properties of the films obtained by LBL assembly change with the number of layers N.[15,24,25,52] For low N, AFM measurements show that the substrate is covered by isolated islands.[53] The layers are then described as thin, porous, hydrated, and containing a relatively large amount of small ions. In the CMM, the electrode surface is visualized as an insulating plane sprinkled with active sites of radius r_a and separated a distance r_b. The decrease in ion permeability with increasing N is attributed to a decrease in the active electrode area and slow diffusion within the film.

The extent to which mass transport to these active regions deviates from linear diffusion depends on the degree of coverage and size of the active sites. For the first layers, $N \leq 6$, the effective coverage θ is low. The active areas have a relatively large radius and can be either uncovered areas or areas covered with only few layers of polyelectrolyte, as illustrated in Figure 2a.

In the transition to the seventh layer, other researchers have noticed that the thickness increase per layer becomes larger and the film becomes more compact.[24,52] We attribute the increase in R_f, C_f, and θ noticed for the three types of films, after the assembly of the seventh layer, to these effects. In particular, we have noticed then that that the impedance increases drastically, the CVs became plateau shaped and there is a strong decrease in the current. These facts are consistent with the kind of active sites suggested for very high coverage, depicted in Figure 2b. The species has to diffuse through the outer layers of the film before reaching one of the previously uncovered "holes". The diffusion coefficients of highly charged species in the film may be several orders of magnitude lower than in the solution and may depend on the number of layers.[27] The lowest values obtained here are of the order of 10^{-9} cm^2 s^{-1}, in agreement with the observations in ref 54. The magnitude of the electric current reflects, therefore, the "true" active area of the electrode and a lower diffusion coefficient.[55]

The EIS measurements in Figures 4−6 agree quite well with the theoretical curves calculated from the equivalent circuit in Figure 10, with Z_d evaluated from eq 1 and the parameter values shown in Tables1−3. In these tables N makes reference to the number of layers added to the cysteamine monolayer. The solution resistance R_s is about 140 Ω for the three polycations used. We assume for the sake of simplicity $K_1 = K_2 = K = 1$ and $D_1^s = D_2^s = D^s = 5.1 \times 10^{-6}$ cm^2 s^{-1}.[29] In this model, the apparent charge-transfer resistance is

$$R_{CT}^{(app)} = \frac{R_{CT}}{1-\theta} \tag{6}$$

where the measured charge-transfer resistance R_{CT} for bare gold was ca. 100 Ω.

The Nyquist diagrams for $N \leq 6$ show a straight line of approximately unit slope at low frequencies, meaning that diffusion is linear in this frequency range (insets of Figures 4−6). The diffusion layers of neighboring active regions overlap at high frequencies. The diagrams for $N \geq 7$ show a deviation from a straight line of unit slope at low frequencies, indicating nonlinear diffusion. This different behavior for thick and thin films is also observed in the CVs (Figures 7−9). For $N \leq 6$, the shape of the CVs is rather similar to that of the bare electrode and the peak currents are almost the same. For $N \geq 7$, the film heterogeneities are important and the CVs differ significantly from those of a homogeneous electrode surface. In the time scale of the CVs, there is practically no overlap of the diffusion profiles to neighboring capillaries[50,51] and diffusion is nonlinear. The CVs become more plateau-shaped and the peak currents decrease due to the effect of both the reduction of the diffusion coefficient in the film and the nonlinear diffusion. Moreover, the small increase in peak separation in the CVs with increasing N is attributed to an increase in θ that in turn increases the charge-transfer resistance $R_{CT}^{(app)}$, as shown in eq 7.

The parameter values in Tables 1−3 (obtained from the fittings) show that for $N \leq 6$ the overall trend of the film capacitance C_f is to increase with the number of layers. This

TABLE 1: Parameter Values Obtained by Fitting the Impedance Data of the pSS/pHis films to the Equivalent Circuit Represented in Figure 10 with the Diffusion Impedance Given by Eq 1[a]

N	C_f (μF)	R_f (kΩ)	C_{dl} (μF)	θ	r_a (μm)	R_m (kΩ)	D_R
1	0.03 ± 0.01	~ 0	0.82 ± 0.09	0.005 ± 0.001	8.0 ± 0.9	∞	1.00 ± 0.01
2	0.053 ± 0.009	0.76 ± 0.02	0.75 ± 0.09	0.20 ± 0.05	7.6 ± 0.9	∞	0.80 ± 0.02
3	0.120 ± 0.006	3.05 ± 0.06	0.50 ± 0.09	0.30 ± 0.06	7.5 ± 0.9	∞	0.40 ± 0.02
4	0.177 ± 0.002	5.4 ± 0.3	0.49 ± 0.09	0.39 ± 0.08	4.5 ± 0.9	110 ± 20	0.20 ± 0.02
5	0.220 ± 0.002	36.2 ± 0.3	0.48 ± 0.09	0.51 ± 0.01	4.5 ± 0.9	65 ± 5	0.05 ± 0.02
6	0.240 ± 0.001	31.7 ± 0.2	0.47 ± 0.09	0.58 ± 0.01	3.0 ± 0.5	43 ± 1	0.025 ± 0.003
7	0.135 ± 0.002	72.8 ± 0.4	0.33 ± 0.05	0.47 ± 0.01	3.2 ± 0.4	480 ± 10	0.0030 ± 0.0001
8	0.260 ± 0.005	168 ± 1	0.99 ± 0.03	0.900 ± 0.001	4.2 ± 0.5	∞	0.0042 ± 0.0002
9	0.350 ± 0.003	168 ± 8	0.99 ± 0.03	0.910 ± 0.001	4.2 ± 0.5	∞	0.0042 ± 0.0002
10	0.360 ± 0.004	265 ± 2	0.99 ± 0.04	0.940 ± 0.001	4.5 ± 0.5	∞	0.0042 ± 0.0002

[a] Values are given for the 95% confidence bounds of the parameters.

TABLE 2: Same as Table 1 for PSS/PLys Films

N	C_f (μF)	R_f (kΩ)	C_{dl} (μF)	θ	r_a (μm)	R_m (kΩ)	D_R
1	0.035 ± 0.009	~ 0	1.2 ± 0.2	0.005 ± 0.002	9 ± 1	∞	1.00 ± 0.01
2	0.10 ± 0.01	~ 0	1.2 ± 0.2	0.05 ± 0.01	5.8 ± 0.9	∞	1.00 ± 0.01
3	0.140 ± 0.003	1.00 ± 0.04	0.8 ± 0.1	0.18 ± 0.04	8.6 ± 0.9	∞	1.00 ± 0.04
4	0.193 ± 0.009	0.45 ± 0.02	0.95 ± 0.09	0.10 ± 0.02	9.5 ± 0.9	∞	0.85 ± 0.04
5	0.292 ± 0.009	6.00 ± 0.05	0.75 ± 0.09	0.45 ± 0.02	12 ± 3	∞	0.70 ± 0.04
6	0.200 ± 0.004	1.70 ± 0.03	0.43 ± 0.06	0.45 ± 0.03	4.0 ± 0.9	∞	0.45 ± 0.06
7	0.200 ± 0.004	24.8 ± 0.2	0.92 ± 0.08	0.49 ± 0.02	0.20 ± 0.05	41 ± 2	0.002 ± 0.002
8	0.270 ± 0.002	16.2 ± 0.4	0.20 ± 0.03	0.72 ± 0.02	3.8 ± 0.3	65 ± 2	0.044 ± 0.002
9	0.300 ± 0.001	48.0 ± 0.1	0.90 ± 0.03	0.20 ± 0.09	0.20 ± 0.05	73 ± 2	0.0016 ± 0.0003
10	0.440 ± 0.009	29.0 ± 0.3	0.94 ± 0.06	0.55 ± 0.02	0.32 ± 0.05	60 ± 5	0.0016 ± 0.0002

TABLE 3: Same as Table 1 for PSS/PArg Films

N	C_f (μF)	R_f (kΩ)	C_{dl} (μF)	θ	r_a (μm)	R_m (kΩ)	D_R
1	0.04 ± 0.01	~0	1.2 ± 0.1	0.005 ± 0.002	9 ± 3	∞	1.00 ± 0.01
2	0.07 ± 0.01	~0	1.2 ± 0.1	0.003 ± 0.002	10 ± 3	∞	0.50 ± 0.01
3	0.150 ± 0.005	0.38 ± 0.01	1.1 ± 0.1	0.10 ± 0.02	9 ± 1	∞	1.00 ± 0.01
4	0.160 ± 0.006	0.38 ± 0.01	1.0 ± 0.1	0.12 ± 0.02	10 ± 1	∞	0.80 ± 0.01
5	0.280 ± 0.002	6.60 ± 0.06	0.51 ± 0.09	0.46 ± 0.04	8.8 ± 0.9	∞	0.60 ± 0.03
6	0.260 ± 0.003	5.20 ± 0.07	0.31 ± 0.09	0.59 ± 0.02	4.0 ± 0.3	∞	0.25 ± 0.04
7	0.230 ± 0.002	103.0 ± 0.6	0.23 ± 0.09	0.75 ± 0.03	4.2 ± 0.4	690 ± 80	0.012 ± 0.002
8	0.230 ± 0.002	140.0 ± 0.3	0.30 ± 0.05	0.75 ± 0.05	4.8 ± 0.6	690 ± 80	0.0058 ± 0.0003
9	0.320 ± 0.005	210 ± 1	0.80 ± 0.08	0.9 ± 0.1	3.0 ± 0.4	∞	0.0022 ± 0.0002
10	0.250 ± 0.002	174 ± 1	0.90 ± 0.08	0.81 ± 0.07	6.5 ± 0.9	∞	0.0049 ± 0.0003

may reflect that the film area is increasing. Conversely the decrease in exposed metal area explains the decrease in the double layer capacitance C_{dl}.[50] For $N \geq 7$, the geometries to be considered are those of the covered pinholes (i.e., the hollow regions within the film) and the trends depend strongly on each particular polycatio and on how the internal layers are affected from the deposition of the external ones. This is only significant during the transition to a more compact multilayer. C_{dl} is always higher than C_f, as expected.[46]

The change in the high-frequency semicircle of the Nyquist diagrams with N is mainly due to the increase in R_f. The film resistance becomes detectable immediately after the second or third layers and the values obtained are of the same order of magnitude as those reported by other researchers.[47] The film resistance of pSS/pHis and pSS/pArg films is higher than that of pSS/pLys films, which agrees with the conclusion drawn from the FT-IRRAS measurements that the former ones (and specially pSS/pHis films) contain a higher mass of polyelectrolyte deposited. In relation to the variation of R_f with N, it is observed that it increases nonlinearly with N for the pSS/pHis films but decreases with N for the pLys-terminated films. This is thought to be due to the fact that pLys enhances the permeant ion content in the film, as indicated by the values of the effective coverage discussed below.

We have mentioned above that the decrease in ion permeability with increasing N is attributed to a decrease in D_R and in the active electrode area r_a, and to an increase in the coverage θ. For the pSS/pHis and pSS/pArg films, θ increases monotonically with N, whereas for the pSS/pLys it depends on the charge of the last deposited layer. The assembly of a pLys layer decreases the effective blockage, and the radius of the active areas increases. This may be interpreted considering again that this film is the one for which the polyelectrolyte mass deposited in each step is lowest. This probably results in thinner, less dense layers, and therefore the penetration of the electroactive ion through areas covered with only a few layers is enhanced, due to electrostatic attraction, when pLys is the terminal layer. Thus, as far as blocking is concerned, the outer pLys plays a minor role. Actually, because the charge of the previous pSS layer is overcompensated, the blocking effect of this layer can be surmounted too. The result is an effective coverage that differ substantially from the truly coated area for pLys-terminated films. This helps to explain why these films exhibit smaller impedances and larger currents than the previous pSS-terminated ones. In the case of the pSS/pArg films, despite the expected high positive charge density exhibited by polycation-terminated films ($pK_a \sim 12$), the possible penetration through areas covered by a small number of layers due to electrostatic attraction may be prevented by the thickness of the layers. For a pSS/pHis film, this effect is particularly important because, as suggested by the FT-IRRAS measurements, it has the largest amount of polyelectrolyte deposition among the films studied. Additionally, because the electrochemical measurements were carried out in a neutral medium, it is expected that the positive charge density

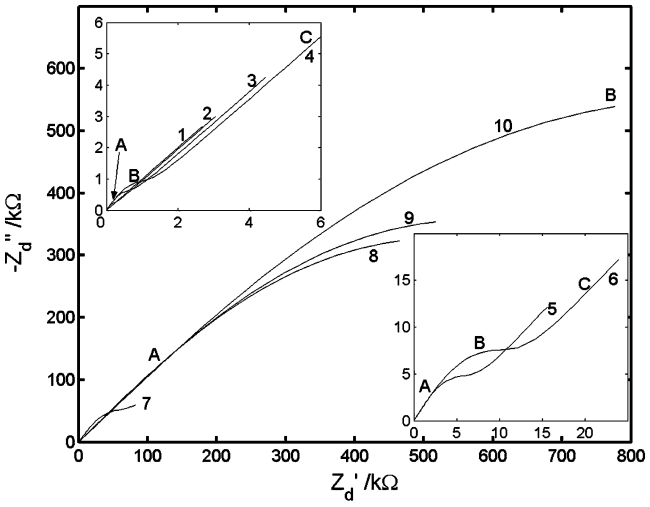

Figure 11. Nyquist diagrams of the simulated diffusion impedances corresponding to Figure 4. The letters indicate the regions of different diffusion behavior as explained in the text.

exhibited by the pHis-terminated films to be less than that of a pLys or pArg-terminated film, because the pK_a of the histidine residues is approximately 7. The combination of these two effects may explain why the pHis/pSS films are the ones having the higher effective coverage and, thus, higher impedances.

In Figure 11 the diffusion impedance Z_d is represented in the complex plane. The spectra for $N \leq 6$ show three regions.[33,50,51] At high frequencies (region A) the diffusion layer thickness δ is small compared to the size of the active areas and the distance between them, $\delta \gg r_a$, r_b, the diffusion profiles do not overlap and semi-infinite linear diffusion to each active area is observed (slope ca. 1 in the Nyquist plot). At intermediate frequencies (region B) the diffusion layer thickness increases so that $r_a < \delta < r_b$ and nonlinear diffusion to the active sites occurs. At low frequencies the individual diffusion profiles merge into a global one and semi-infinite linear diffusion is again expected, this time corresponding to the entire geometric area of the electrode (region C). The width of the frequency interval corresponding to regions A, B, and C varies with the number of layers N. With increasing N, the frequency at which the individual diffusion profiles overlap decreases, and for $N > 7$only region A is seen in the spectra.

As a final observation, we mention that in our model the decreased permeability with the number of layers is the result of mass transport limitations only.[26] On the contrary, other researchers have suggested, on the basis of an analysis of the EIS results using the Randles circuit[23−25] that the electroactivity seems to be limited by electron transfer-kinetics under some conditions and in the films they studied.

II. Homogeneous Membrane Model (HMM). In Figure 12 the experimental impedance spectra is represented for different numbers of layers of the pSS/pHis film against the one calculated using the diffusion impedance from the HMM.[26−28] The apparent charge-transfer resistance in this model is

$$R_{CT}^{(app)} = \frac{R_{CT}}{K} \tag{7}$$

The agreement between the experimental and the HMM theoretical results is not so good as that obtained with the CMM, whose predictions are also shown in Figure 11 for comparison (notice that in the curves for the HMM model K is considered to be different from unity). Similar results were obtained for the other two films.

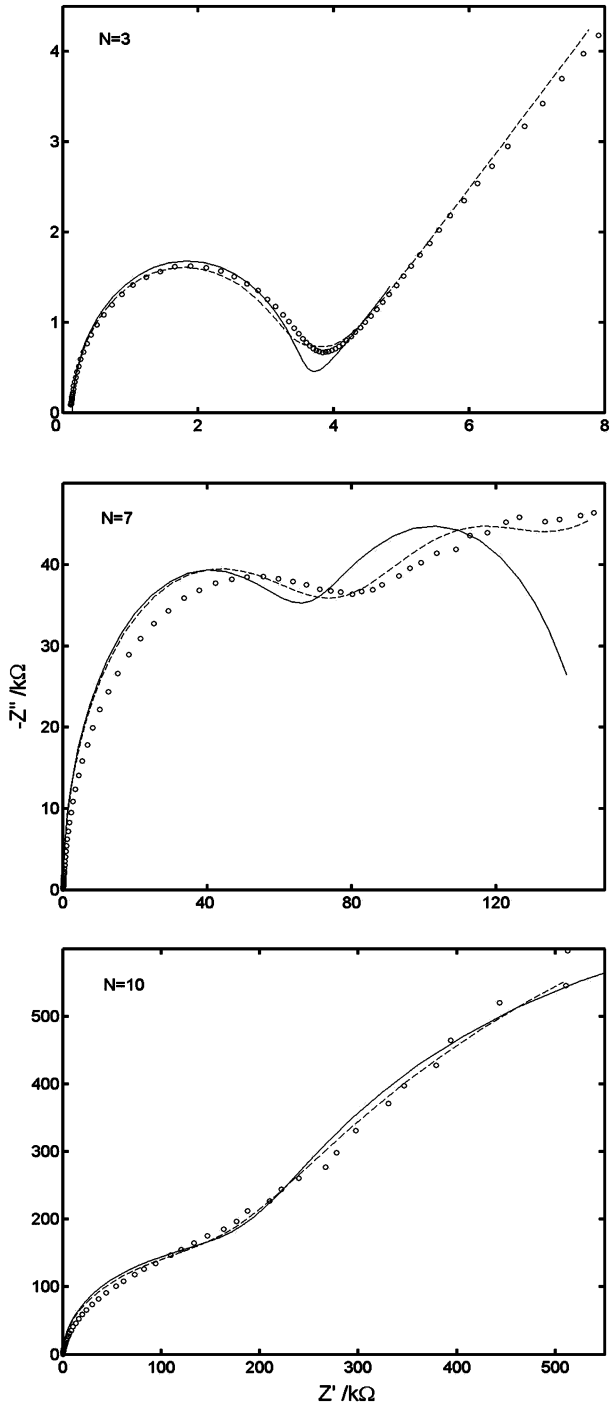

Figure 12. Impedance spectra of pSS/pHis films for different numbers of layers N, including experimental data (circles), theoretical results from HMM (solid lines) and theoretical results from CMM (dotted lines, parameter values from Table 1). The parameter values used in the HMM are $L/N = 3$ nm, $C_f = 1.00$ μF, $C_{dl} = 1.20$ μF, $R_f = 3.1$ kΩ, $R_m = \infty$, $D^f = 9.1 \times 10^{-8}$ cm^2 s^{-1}, $K = 0.4$ for $N = 3$; $C_f = 0.39$ μF, $C_{dl} = 6.20$ μF, $R_f = 78.0$ kΩ, $R_m = 360$ kΩ, $D^f = 5.3 \times 10^{-9}$ cm^2 s^{-1}, $K = 0.020$ for $N = 7$; $C_f = 0.41$ μF, $C_{dl} = 1.70$ μF, $R_f = 270$ kΩ, $R_m = \infty$, $D^f = 2.5 \times 10^{-10}$ cm^2 s^{-1}, $K = 0.039$ for $N = 10$.

We may suggest that the better account of the experimental results given by the CMM compared to the HMM may be associated with the fact that the first probes the existence of preferential paths for transport of highly charged ions across the film due to a rough substrate or even due to the mechanism of multilayer growth.[53] Because the effect of these irregularities decays as the number of layers in the film increases, the HMM can be applied satisfactorily only in very thick films (N large).

Conclusion

We have discussed two transport models, the CMM and the HMM, for a polyelectrolyte multilayer assembled onto alkanethiol-modified gold surfaces and validated them using EIS and CV data obtained for three different films. The decrease in the permeability with the number of layers N, for these films (and for $N < 11$), seems to be associated with a progressive reduction in the active area of the film/electrode. The agreement between the experimental results and the impedance calculations from the CMM is quite good for all films studied. On the contrary, the HMM gives a rather poor account of the experimental trends. According to the CMM the variations noticed in the EIS spectra, peak current intensities and CV shape are attributed to variations in the active area and size of the active sites with the number of layers. The nature of the active sites may also vary, so that after a certain number of layers the slow diffusion in the film begins to be dominant. We point out that the active sites do not have to be bare electrode areas but merely spots on the film surface through which transport is preferentially made relative to the remaining film surface.

Acknowledgment. This research is partially funded by the Portuguese government through the Fundação para a Ciência e a Tecnologia (FCT) CIQ-L4. S.V.P.B. acknowledges FCT for a Ph.D. grant. J.A.M. and V.G.M. are thankful for the financial support from the Ministry of Science and Technology of Spain and the European Funds for Regional Development (FEDER) under project number MAT2002-00646. Financial support by the EU under the research and training network SUSANA (HPRN-CT-2002-00185), is also gratefully acknowledged.

Appendix

The homogeneous membrane model for the multilayer has been considered by Schlenoff et al.,[26−28] but to the best of our knowledge an explicit expression for the concentration impedance has not been presented previously. We derive here eq 5. The concentration of species k, $c_k^i(x,t)$, depends on the distance x to the metal electrode and time t. Superscript i denotes the spatial region (s for the external solution; f for the film). Its diffusion coefficient in the film D_k^f may be considerably smaller than that in the external solution, D_k^s.

We aim at solving Fick's equation

$$\frac{\partial c_k^i}{\partial t} = D_k^i \frac{\partial^2 c_k^i}{\partial x^2} \tag{A1}$$

for two homogeneous diffusion media in series. At the membrane−solution interface the flux density is continuous and electrochemical equilibrium is established so that

$$D_k^s \left.\frac{\partial c_k^s}{\partial x}\right|_{x=L} = D_k^f \left.\frac{\partial c_k^f}{\partial x}\right|_{x=L} \tag{A2}$$

$$c_k^f(L,t) = K_k c_k^s(L,t) \tag{A3}$$

At the electrode surface, Faraday's law requires that

$$\frac{I_k(t)}{nFA} = D_k^f \left.\frac{\partial c_k^f}{\partial x}\right|_{x=0} \tag{A4}$$

The initial concentration profiles in the film and the external solution are independent of x. Equation A3 is satisfied throughout the film.

Equations A1−A4 can be solved using Laplace transforms and lead to

$$\bar{c}_k^f(x,s) = \frac{c_k^f(x,0)}{s} + A_k(s)e^{\sqrt{s/D_k^f}x} + B_k(s)e^{-\sqrt{s/D_k^f}x} \tag{A5}$$

where, if we replace s by $j\omega$,[54,56]

$$A_k = \frac{\bar{I}_k(s)e^{-a_k\sqrt{\omega}}}{2nFA\sqrt{D_k^f j\omega}} \frac{1-b_k}{\cosh(a_k\sqrt{\omega}) + \sqrt{D_R}\sinh(a_k\sqrt{\omega})} \tag{A6}$$

$$B_{kI} = \frac{\bar{I}_k(s)e^{a_k\sqrt{\omega}}}{2nFA\sqrt{D_k^f j\omega}} \frac{1+b_k}{\cosh(a_k\sqrt{\omega}) + \sqrt{D_R}\sinh(a_k\sqrt{\omega})} \tag{A7}$$

$$a_k = \frac{L}{\sqrt{2D_k^f}}(1+j) \tag{A8}$$

$$b_k = K_k\sqrt{D_R} \tag{A9}$$

The contribution of species k to the concentration impedance is then

$$Z_{k,d}^{(m)} = \frac{\sigma_k^{(m)}}{\sqrt{j\omega}} \frac{\tanh(a_k\sqrt{\omega}) + b_k}{1 + b_k\tanh(a_k\sqrt{\omega})} \tag{A10}$$

where

$$\sigma_k^{(m)} = \frac{RT}{n^2F^2A\sqrt{2D_k^f c_k^f(0)}} \tag{A11}$$

and, hence, the total concentration impedance is given by eq 5.

Supporting Information Available: FT-IRRAS band assignments. This material is available free of charge via the Internet at http://pubs.acs.org.

References and Notes

(1) Groth, T.; Lendlein, A. *Angew. Chem., Int. Ed.* **2004**, *43*, 926−928.
(2) Jin W.; Toutianoush, A.; Tieke, B. *Langmuir* **2003**, *19*, 2550−2553.
(3) Kidambi, S.; Dai, J.; Li, J.; Bruening, M. L. *J. Am. Chem. Soc.* **2004**, *126*, 2658−2659.
(4) Li, W.; Hooks, D. E.; Chiarelli, P.; Jiang, Y.; Xu, H.; Wang, H.-L. *Langmuir* **2003**, *19*, 4639−4644.
(5) Georgieva, R.; Moya, S.; Donath, E.; Bäumler, H. *Langmuir* **2004**, *20*, 1895−1900.
(6) Berg, M. C.; Yang, S. Y.; Hammond, P. T.; Rubner, M. F. *Langmuir* **2004**, *20*, 1362−1368.
(7) Farhat, T. R.; Schlenoff, J. B. *Electrochem. Solid State Lett.* **2002**, *5*, B13−B15.
(8) Barreira, S. V. P.; Silva, F. *Langmuir* **2003**, *19*, 10324−10331.
(9) Jiang, S.; Liu, M. *J. Phys. Chem. B* **2004**, *108*, 2880−2884.
(10) Hoogeveen, N. G.; Stuart, M. A. C.; Fleer, G. J. *Langmuir* **1996**, *12*, 3675−3681.
(11) Schlenoff, J. B.; Dubas, S. T. *Macromolecules* **2001**, *34*, 592−598.
(12) Schwarz B.; Schönhoff, M. *Langmuir* **2002**, *18*, 2964−2966.
(13) Steitz, R.; Jaeger, W.; Klitzing, R. v. *Langmuir* **2001**, *17*, 4471−4474.
(14) Glinel, K.; Moussa, A.; Jonas, A. M.; Laschewsky, A. *Langmuir* **2002**, *18*, 1408−1412.
(15) Decher, G. *Science* **1997**, *277*, 1232−1237.
(16) Shiratori, S. S.; Rubner, M. F. *Macromolecules* **2000**, *33*, 4213−4219.
(17) Dubas, S. T.; Schlenoff, J. B. *Macromolecules* **2001**, *34*, 3736−3740.

(18) Voigt, U.; Jaeger, W.; Findenegg, G. H.; Klitzing, R. v. *J. Phys. Chem. B* **2003**, *107*, 5273−5280.
(19) Krasemann, L.; Tieke, B. *Langmuir* **2000**, *16*, 287−290.
(20) Lebedev, K.; Ramírez, P.; Mafé, S.; Pellicer, J. *Langmuir* **2000**, *16*, 9941−9943.
(21) Antipov, A. A.; Sukhorukov, G. B.; Möhwald, H. *Langmuir* **2003**, *19*, 2444−2448.
(22) Nicol, E.; Habib-Jiwan, J.-L.; Jonas, A. M. *Langmuir* **2003**, *19*, 6178−6186.
(23) Han, S.; Lindholm-Sethson, B. *Electrochim. Acta* **1999**, *45*, 845−853.
(24) Harris, J. J.; Bruening, M. L. *Langmuir* **2000**, *16*, 2006−2013.
(25) Pardo-Yissar, V.; Katz, E.; Lioubashevski, O.; Willner, I. *Langmuir* **2001**, *17*, 1110−1118.
(26) Farhat, T. R.; Schlenoff, J. B. *Langmuir* **2001**, *17*, 1184−1192.
(27) Farhat, T. R.; Schlenoff, J. B. *J. Am. Chem. Soc.* **2003**, *125*, 4627−4636.
(28) Rmaile, H. H.; Farhat, T. R.; Schlenoff, J. B. *J. Phys. Chem. B* **2003**, *107*, 14401−14406.
(29) Geshi, T.; Tokuda, K.; Matsuda, H. *J. Electroanal. Chem.* **1978**, *89*, 247−260.
(30) Geshi, T.; Tokuda, K.; Matsuda, H. *J. Electroanal. Chem.* **1979**, *101*, 29−38.
(31) Tokuda, K.; Geshi, T.; Matsuda, H. *J. Electroanal. Chem.* **1979**, *102*, 41−48.
(32) Amatore, C.; Savéant, J. M.; Tessier, D. *J. Electroanal. Chem.* **1983**, *147*, 39−51.
(33) Finklea, H. O.; Snider, D. A.; Fedyk, J.; Sabatani, E.; Gafni, Y.; Rubinstein, I. *Langmuir* **1993**, *9*, 3660−3667.
(34) Brookes, B. A.; Davies, T. J.; Fisher, A. C.; Evans, R. G.; Wilkins, S. J.; Yunus, K.; Wadhawan, J. D.; Compton, R. G. *J. Phys. Chem. B* **2003**, *107*, 1616−1627.
(35) Hubrecht, J.; Embrechts, M.; Bogaerts, W. *Electrochim. Acta* **1993**, *38*, 1867−1875.
(36) Diao, P.; Guo, M.; Tong, R. *J. Electroanal. Chem.* **2001**, *495*, 98−105.
(37) Protsailo, L. V.; Fawcett, W. R. *Langmuir* **2002**, *18*, 8933−8941.
(38) Porter, M. D.; Bright, T. B.; Allara, D. L.; Chidsey, C. E. D. *J. Am. Chem. Soc.* **1987**, *109*, 3559−3568.
(39) Ulman, A. *Chem. Rev.* **1996**, *96*, 1533−1554.
(40) Schlenoff, J. B.; Ly, H.; Li, M. *Langmuir* **1998**, *120*, 7626−7634.
(41) Kim, B. Y.; Bruening, M. L. *Langmuir* **2003**, *19*, 94−99.
(42) Kotov, N. A. *Nanostruct. Mater.* **1999**, *12*, 789−796.
(43) Creighton, T. E. *Proteins, Structures and molecular properties*; Freeman: New York, 1984.
(44) Slevin, C. J.; Mälkiä, A.; Liljeroth, P.; Toiminen, M.; Kontturi, K. *Langmuir* **2003**, *19*, 1287−1294.
(45) Liu, Y.; Zhao, M.; Bergbreiter, D. E.; Crooks, R. M. *J. Am. Chem. Soc.* **1997**, *119*, 8720−8721.
(46) Amirudin, A.; Thierry, D. *Prog. Org. Coat.* **1995**, *26*, 1−28.
(47) Harris, J. J.; DeRose, P. M.; Bruening, M. L. *J. Am. Chem. Soc.* **1999**, *121*, 1978−1979.
(48) Boubour, E.; Lennox, R. B. *Langmuir* **2000**, *16*, 7464−7470.
(49) Durstock, M. F.; Rubner, M. F. *Langmuir* **2001**, *17*, 7865−7872
(50) Sabatani, E.; Cohen-Boulakia, J.; Bruening, M.; Rubinstein, I. *Langmuir* **1993**, *9*, 2974−2981.
(51) Sabatani, E.; Rubinstein, I. *J. Phys. Chem.* **1987**, *91*, 6663−6669
(52) Ladam, G.; Schaad, P.; Voegel, J. C.; Schaaf, P.; Decher, G.; Cuisinier, F. *Langmuir* **2000**, *16*, 1249−1255.
(53) Picart, C.; Lavalle, Ph.; Hubert, P.; Cuisinier, F. J. G.; Decher, G.; Schaaf, P.; Voegel, J.-C. *Langmuir* **2001**, *17*, 7414−7424.
(54) Dai, J.; Balachandra, A. M.; Lee, J. I.; Bruening, M. L. *Macromolecules* **2002**, *35*, 3164−3170.
(55) Che, G.; Li, Z.; Zhang, H.; Cabrera, C. R. *J. Electroanal. Chem.* **1998**, *453*, 9−17.
(56) Girault, H. H. *Electrochimie physique et analytique*; Presses polytechniques et universitaires romandes: Lausanne, 2001.